Available online at www.sciencedirect.com
SCIENCE DIRECT
Journal of Power Sources 156 (2006) 620–628
JOURNAL OF POWER SOURCES
www.elsevier.com/locate/jpowsour

Review of models for predicting the cycling performance of lithium ion batteries

Shriram Santhanagopalan [1], Qingzhi Guo [1], Premanand Ramadass [2], Ralph E. White [*,3]

Center for Electrochemical Engineering, Department of Chemical Engineering, University of South Carolina, Columbia, SC 29208, USA

Received 19 April 2005; accepted 6 May 2005
Available online 12 July 2005

Abstract

A rigorous pseudo two-dimensional model to simulate the cycling performance of a lithium ion cell is compared with two simplified models. The advantage of using simplified models is illustrated and their limitations are discussed. It is shown that for 1*C* or less discharge rates a simple ordinary differential equation (ODE) model can be used to predict accurately the potential as a function of time. For rates higher than 1*C*, simplifications to the rigorous model are suggested that reduce the solution time for the model.

Keywords: Lithium ion batteries; Model; Cycling

1. Introduction

The literature on modeling of lithium ion batteries is quite extensive [1–4]. The first model with two composite electrodes and a separator was presented by Fuller et al. [5] Simplified models were presented by Doyle and Newman [6] to develop design correlations under limiting cases. Analytic expressions for the specific capacity against discharge rate were also presented by these authors [7]. The model presented by Fuller et al. [5] was extended by Ramadass et al. [17] to account for the decay in capacity of the cell with cycle number. A side reaction leading to the formation of a film on the surface of the carbon particles at the anode was proposed to occur during the charging process. The potential drop across the film was expressed as a function of the film thickness, which varied with time in accordance with Faraday's law. The loss of active material due to the side reaction and the resultant additional drop in the anodic overpotential were used to account for the capacity fade in the cell. Further extensions to this model were made by Sikha et al. [8] that included the change in the porosity of the electrode material as a function of time. In all these models, the concentration of lithium within the solid phase was either calculated using the superposition principle [11] or solved for rigorously, using a pseudo second dimension along the radius of the particle. Since the concentration of lithium at the particle surface is the only variable of interest, this methodology is cumbersome and time consuming. A very good approximation of the concentration profile within the solid phase was presented independently by Wang et al. [9] and Subramanian et al. [10] based on the integral approach outlined by Ozisik [11]. In this second approach, the concentration profile within the solid particle is approximated by a second-degree polynomial whose coefficients are expressed in terms of the average concentration of lithium inside the particle and the concentration at the surface. Thus, the need to solve for the concentration profile within the solid phase is elimi-

* Corresponding author. Tel.: +1 803 777 3270; fax: +1 803 777 9597/8265.
E-mail address: white@engr.sc.edu (R.E. White).
[1] Electrochemical Society Student Member.
[2] Electrochemical Society Active Member.
[3] Electrochemical Society Fellow.

0378-7753/$ – see front matter © 2005 Elsevier B.V. All rights reserved.
doi:10.1016/j.jpowsour.2005.05.070

Nomenclature

a_j	specific area of the porous electrode 'j' ($m^2\,m^{-3}$)
A_j	surface area of the electrode 'j' (m^2)
brug	Bruggman's coefficient
c	concentration of lithium ($mol\,m^{-3}$)
$c_{s,j}$	average concentration of lithium in the solid phase of electrode 'j' ($mol\,m^{-3}$)
$\bar{c}_{1,j}$	solid phase concentration of lithium at the surface of the sphere ($mol\,m^{-3}$)
$D_{1,j}$	diffusion coefficient of lithium in the solid phase inside electrode 'j' ($m^2\,s^{-1}$)
$D_{2,\text{eff}}$	effective diffusion coefficient of lithium in the solution phase ($=D_{2,j}\varepsilon_2^{\text{brug}}$) ($m^2\,s^{-1}$)
D_2	diffusion coefficient of lithium in the liquid phase ($m^2\,s^{-1}$)
F	Faraday's constant ($C\,mol^{-1}$)
$i^0_{j,\text{side}}$	exchange current density for the side reaction ($A\,m^{-2}$)
J	applied current (A)
J_j	local volumetric current density for intercalation reaction ($A\,m^{-3}$)
$J_{s,j}$	side reaction current (A)
$J_{s,j}$	local volumetric current density for side reaction ($A\,m^{-3}$)
k	rate constant for electrochemical reaction $(A\,m^{-2}\,mol\,m^{-3})^{(1+\alpha)}$
L	length of the cell (m)
$M_{s,j}$	molecular weight of the side reaction product ($kg\,mol^{-1}$)
r	radial coordinate (m)
R_j	radius of the particle (m)
R_{SEI}	resistance of the film ($\Omega\,m^{-2}$)
R	universal gas constant ($J\,mol\,K^{-1}$)
t	time (s)
T	temperature (K)
U^θ	local equilibrium potential (V) (as described in Appendix A of Ref. [17])
V	cell voltage (V)
x	coordinate across the thickness of the cell (m)
y	scaled radial co-ordinate ($=\frac{r}{R_j}L$) (m)

Greek

α	transfer coefficients of the electrochemical reaction
ε	volume fraction of a phase
ϕ	local potential of a phase (V)
η	over potential driving a reaction (V)
κ	conductivity of the electrolyte ($S\,m^{-1}$) (as described in Appendix A of Ref. [17])
σ_{eff}	effective conductivity of an electrode ($=\sigma\varepsilon_j$) ($S\,m^{-1}$)
σ	conductivity of the electrode ($S\,m^{-1}$)
$\rho_{s,j}$	density of the side reaction product ($kg\,m^{-3}$)
δ_f	film thickness (m)

Subscript

1	solid phase
2	liquid phase
j	$=n$ or p
p	positive electrode
n	negative electrode
s	side reaction property
sep	separator

nated. While most of these models adopt the porous electrode approach, Haran et al. [12] presented a simpler representation of the electrode. This was first presented for the metal hydride system and later extended to the lithium ion system [13,14]. In this model, each electrode is represented by a single spherical particle. This approach is popularly referred to as the single particle model.

Each of the above approaches has some advantages compared to the others as well as demerits. For example, while the porous electrode model has the advantage of providing a sophisticated account of the various physical processes occurring in a battery, solving the model is very time consuming. The simplified single particle model is orders of magnitude faster as shown in this work, however, it does not account for all the physical processes, for example, the solution phase diffusion limitations are ignored, thus the validity of the model is limited. Incorporation of the polynomial approximations [9–11] of the solid phase concentration of lithium in the porous electrode models preserves their sophistication while simultaneously reducing the solution time [16]. In simulating the performance of a lithium ion cell over several cycles, the battery model has to be solved repeatedly during each cycle. Ideally, one would expect for such occasions that the model is not time consuming and that it will provide a realistic portrait of the physical processes that occur during cycling. In this context, two simplified models are compared to the rigorous pseudo two-dimensional model in terms of their accuracy in simulating the cycling performance and the time required for their solution.

2. Model equations

The three approaches considered in this study are the rigorous pseudo two-dimensional model (or the P2D model), the single particle model (or the SP model) and the porous electrode model with the polynomial approximation (or the PP

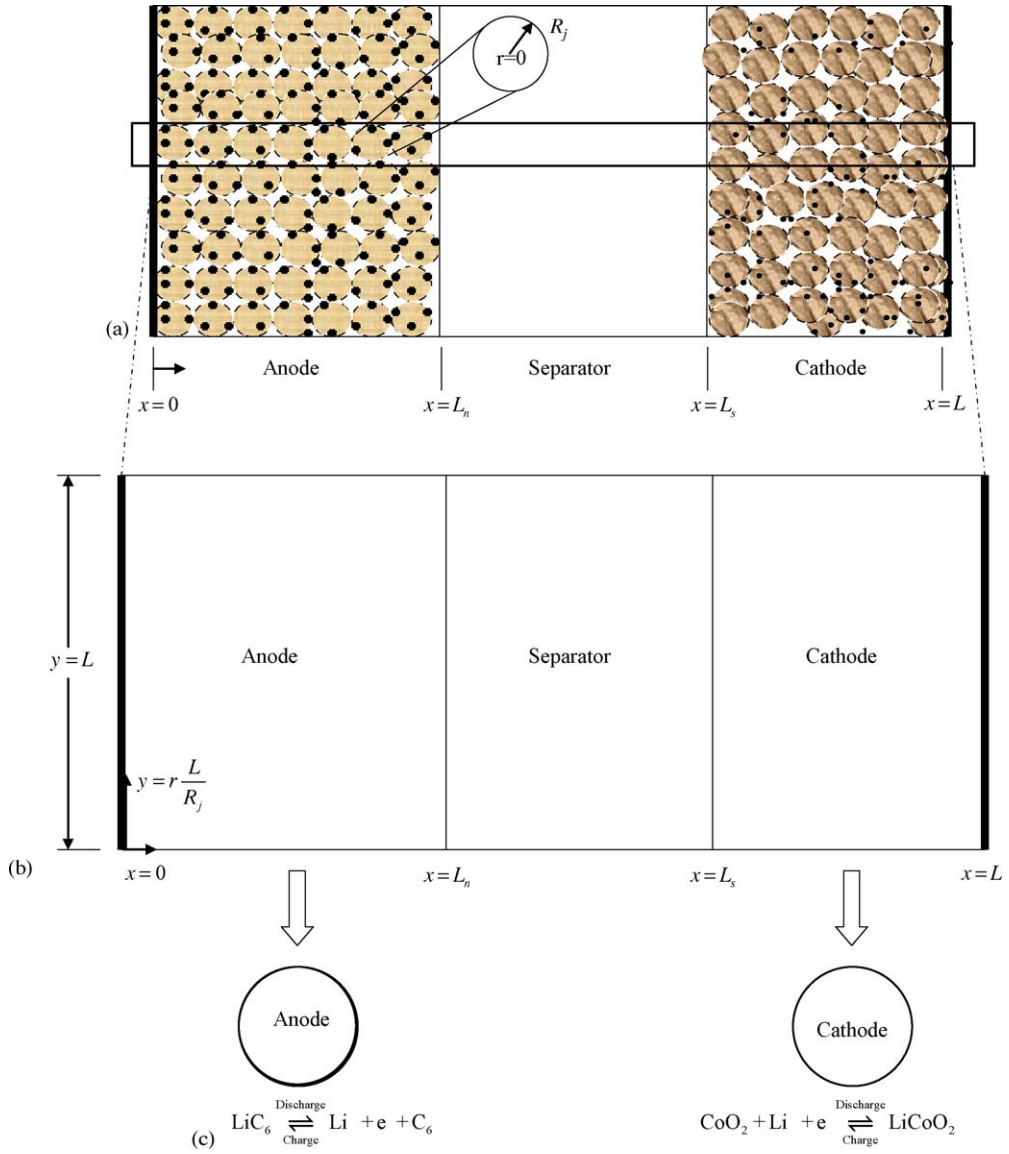

Fig. 1. Simplification of the rigorous two-dimensional model (a) to the pseudo two-dimensional (P2D) model (b) and the single particle (SP) model (c).

model). A detailed description of the underlying assumptions in each model and the set of equations used are elaborated in this section.

2.1. The pseudo 2D model

In this approach, the equations developed by Fuller et al. [5] were modified to include capacity fade. The discussion presented here follows the model developed by Ramadass et al. [17]. The solid phase is assumed to comprise of identical spherical particles of a predetermined size and diffusion in the radial direction is assumed to be the predominant mode of transport. The solution phase concentration and the potentials were assumed to vary only in the 'x' coordinate, as shown in Fig. 1(a). The reduction of the solvent (ethylene carbonate) is assumed to occur in addition to the intercalation of lithium in the carbon electrode during the charging process. The entire contribution to the capacity fade is assumed to be from this reaction. This reaction is assumed to have a constant open circuit potential of 0.4 V versus Li/Li$^+$ and the products of this reaction are assumed to form a film of known conductivity over the carbon particles. As a result of this side reaction, a part of the flux that enters the carbon particle is lost irreversibly, resulting in a decrease of the actual capacity of the cell. Further assumptions regarding the mechanism of capacity fade and their validity are discussed by Ramadass [20]. The governing equations for this model are very similar to those presented by Fuller et al. [5] except for that, the flux at the anode is split into two components: one for the intercalation reaction (J_n) and another for the side reaction ($J_{s,n}$). The thickness of the film formed on the carbon particles is related to the side reaction flux by

Faraday's law as:

$$\frac{\partial \delta}{\partial t} = -\frac{J_{s,n} M_{s,n}}{a_n \rho_{s,n} F} \tag{1}$$

where δ is the thickness of the film. The resistance of this film results in an additional contribution to the overpotential at the anode. Following Ramadass et al. [17] no side reaction at the cathode is considered. Hence, the overpotential (η_n) for the anode (the negative electrode) is given by:

$$\eta_n = \phi_1 - \phi_2 - U_n^{\theta} - \frac{(J_n + J_{s,n})\delta}{a_n \kappa} \tag{2}$$

while that for the cathode is given by:

$$\eta_p = \phi_1 - \phi_2 - U_p^{\theta} \tag{3}$$

The diffusion inside the solid phase is represented by the Fick's laws as:

$$\frac{\partial c_{1,j}}{\partial t} = D_{1,j} \frac{1}{r^2} \frac{\partial}{\partial r} \left(r^2 \frac{\partial c_{1,j}}{\partial r} \right) \tag{4}$$

where $c_{1,j}$ denotes the concentration of lithium inside the solid in the electrode 'j' and $D_{1,j}$ the corresponding diffusion coefficient.

The solution of the set of equations for this rigorous model involves two different length scales: the thickness of the cell (L) is several orders of magnitude higher than the average radius (R_j) of the particles that constitute the electrode. Quite often the numerical instabilities that arise due to the presence of two or more length scales are circumvented by the use of appropriate scaling [15,18,19]. In the present case, the methodology outlined in Appendix E of Ramadass [20] was employed and the radial coordinate was scaled as follows:

$$y = r \frac{L}{R_j} \tag{5}$$

and the scaled radial coordinate is termed as 'y' (See Fig. 1b). In the solution of this rigorous model (see equations in Table 1), the concentration of lithium inside the solid phase ($c_{1,j}$) is solved for at each node point along the 'y' coordinate and the value at $y = L$ is used in the kinetic expressions for representing the surface concentration $\bar{c}_{1,j}$. Further details about this model are presented in Appendices A and B of Ramadass et al. [17].

2.2. The single particle model

In the second approach, the single particle model [12–14] is considered. Each electrode is represented by a single spherical particle whose area is equivalent to that of the active area of the solid phase in the porous electrode. A schematic of this model is provided in Fig. 1c. This model assumes that the limitations posed by the solution phase of the cell are negligible. Hence, the solution phase is not considered while developing the model equations. For example, ϕ_2 are set to zero in Eqs. (2) and (3). The assumptions regarding the side reaction are maintained in this approach as well. This

Table 1
List of equations used for the various models

Variable	P2D model	PP model	SP model
$\phi_{1,j}$	$\nabla \cdot (\sigma_{j,\text{eff}} \nabla \phi_{1,j}) - (J_j + J_{s,j}) = 0$	$\nabla \cdot (\sigma_{j,\text{eff}} \nabla \phi_{1,j}) - (J_j + J_{s,j}) = 0$	$J \mp^{*} J_{s,j} \pm^{**} A_j k_j F (c_{1,j}^{\max} - \bar{c}_{1,j})^{1/2} \bar{c}_{1,j}^{1/2} c_2^{1/2}$
ϕ_2	$\nabla \cdot (\sigma_{j,\text{eff}} \nabla \phi_{1,k}) + \nabla \cdot (\kappa_{\text{eff}} \nabla \phi_2) + \nabla \cdot (\kappa_D \nabla \ln c_2) = 0$	$\nabla \cdot (\sigma_{j,\text{eff}} \nabla \phi_{1,k}) + \nabla \cdot (\kappa_{\text{eff}} \nabla \phi_2) + \nabla \cdot (\kappa_D \nabla \ln c_2) = 0$	$\left\{ \exp\left(\frac{\alpha_a F}{RT} \eta_j\right) - \exp\left(\frac{\alpha_c F}{RT} \eta_j\right) \right\} = 0$
J_j	$J_j = a_j k_j (c_{1,j}^{\max} - \bar{c}_{1,j})^{1/2} \bar{c}_{1,j}^{1/2} c_2^{1/2} \left\{ \exp\left(\frac{\alpha_a F}{RT} \eta_j\right) - \exp\left(-\frac{\alpha_c F}{RT} \eta_j\right) \right\}$	$J_j = a_j k_j (c_{1,j}^{\max} - \bar{c}_{1,j})^{1/2} \bar{c}_{1,j}^{1/2} c_2^{1/2} \left\{ \exp\left(\frac{\alpha_a F}{RT} \eta_j\right) - \exp\left(-\frac{\alpha_c F}{RT} \eta_j\right) \right\}$	–
$J_{s,j}$	$J_{s,j} = -a_j i_{j,\text{side}}^{0} \left\{ -\exp\left(-\frac{\alpha_c F}{RT} \eta_j\right) \right\}$	$J_{s,j} = -a_j i_{j,\text{side}}^{0} \left\{ -\exp\left(-\frac{\alpha_c F}{RT} \eta_j\right) \right\}$	$J = I_{\text{app}}$
$\delta_{f,j}$	$\frac{\partial \delta_{f,j}}{\partial t} = -\frac{J_{s,j} M_{s,j}}{a_j \rho_{s,j} F}$	$\frac{\partial \delta_{f,j}}{\partial t} = -\frac{J_{s,j} M_{s,j}}{a_j \rho_{s,j} F}$	$J_{s,j} = -A_j i_{j,\text{side}}^{0} \left\{ -\exp\left(-\frac{\alpha_c F}{RT} \eta_j\right) \right\}$
$c_{1,j}^{\text{avg}}$	–	$\frac{\partial c_{s,j}}{\partial t} + \frac{15 D_{1,j}}{R_j^2} (c_{s,j} - \bar{c}_{1,j}) = 0$	$\frac{\partial \delta_{f,j}}{\partial t} = -\frac{J_{s,j} M_{s,j}}{A_j \rho_{s,j} F}$
$\bar{c}_{1,j}$	$\frac{\partial c_{1,j}}{\partial t} = \frac{D_{1,j}}{r^2} \frac{\partial}{\partial r} \left(r^2 \frac{\partial c_{1,j}}{\partial r} \right), \bar{c}_{1,j} = c_{1,j}\vert_{r=R_j}$	$\frac{5 D_{1,j}}{R_j} (\bar{c}_{1,j} - c_{s,j}) + \frac{(J_j + J_{s,j})}{a_j F} = 0$	$\frac{\partial c_{s,j}}{\partial t} + \frac{15 D_{1,j}}{R_j^2} (c_{s,j} - \bar{c}_{1,j}) = 0$
c_2	$\varepsilon_2 \frac{\partial c_2}{\partial t} = \nabla \cdot (D_{2,\text{eff}} \nabla c_2) + \frac{(1 - t^{+})}{F} (J_k + J_{s,k})$	$\varepsilon_2 \frac{\partial c_2}{\partial t} = \nabla \cdot (D_{2,\text{eff}} \nabla c_2) + \frac{(1 - t^{+})}{F} (J_k + J_{s,k})$	$\frac{5 D_{1,j}}{R_j} (\bar{c}_{1,j} - c_{s,j}) + \frac{(J \mp^{*} J_{s,j})}{A_j F} = 0$
			–

*Positive when j = n and negative when j = p.
**Negative when j = n and positive when j = p.

model is further simplified when the concentration within the sphere is approximated by a parabolic profile [9–11]. The solid phase concentration is represented by a second order polynomial whose coefficients are expressed in terms of the average concentration $c_{s,j}$ and the concentration at the surface of the sphere, $\bar{c}_{1,j}$. This reduces Eq. (4) to a first order ODE and an algebraic equation, eliminating the dependence on the spatial variable 'r'. The resultant equations are: [9,10,14]

$$\frac{\partial c_{s,j}}{\partial t} + \frac{15D_{1,j}}{R_j^2}(c_{s,j} - \bar{c}_{1,j}) = 0 \tag{6}$$

$$\frac{5D_{1,j}}{R_j}(\bar{c}_{1,j} - c_{s,j}) + \frac{J_j}{A_j F} = 0 \tag{7}$$

The initial condition to Eq. (6) is:

$$c_{s,j}|_{t=0} = c_{1,j,0} \tag{8}$$

where $c_{1,j,0}$ denotes the concentration of lithium inside electrode 'j' at the beginning of charge or discharge. The surface concentration $\bar{c}_{1,j}$ is then used in the place of $c_{1,j}|_{r=R_j}$ in the flux expressions. For an elaborate derivation of Eqs. (6)–(8) see Subramanian et al. [10].

2.3. The porous electrode model with the polynomial approximation

The third approach considered here involves the incorporation of the parabolic approximation [9–11] into the P2D model. The resultant equations of this approach (the PP approach) retain the complexity of the previous models based on the porous electrode theory, but are mathematically simpler. All assumptions presented for the P2D model hold good for the PP model as well.

In addition to those, in the PP approach it is assumed that the concentration within each spherical particle of each electrode can be approximated with a parabolic profile (similar to the SP model) and as a result, the solution of Eq. (4) at each point along the radial coordinate is now not required. In the set of governing equations for the P2D model, the solid phase concentration ($c_{1,j}$) which was obtained from the solution of Eq. (4) is now replaced with the concentration at the surface ($\bar{c}_{1,j}$) as given by the solution of Eqs. (6)–(8) above. All other equations for the PP approach remain the same as the P2D approach.

The complete set of governing equations for each approach is shown in Table 1. Fig. 1 shows the simplification of the rigorous two-dimensional model to the pseudo two-dimensional model and into the single particle model. The solid phase potential $\phi_{1,n}$ is arbitrarily set to zero at $x = 0$. The other boundary conditions obtained from jump material and charge balances express the continuity of flux across each boundary.

At $x = 0$ and $x = L$:

$$\frac{\partial \phi_2}{\partial x} = 0 \tag{9}$$

$$\frac{\partial c_2}{\partial x} = 0 \tag{10}$$

At $x = L_n$ and L_s:

$$\left(\kappa_{eff}\frac{\partial \phi_2}{\partial x}\right) + \left(\kappa_D \frac{\partial \ln c_2}{\partial x}\right) = 0 \tag{11}$$

At $x = L_n$:

$$\frac{\partial \phi_{1,n}}{\partial x} = 0 \tag{12}$$

$$\left(D_{2,eff}\frac{\partial c_2}{\partial x}\right)_n = \left(D_{2,eff}\frac{\partial c_2}{\partial x}\right)_{sep} \tag{13}$$

At $x = L_s$:

$$\frac{\partial \phi_{1,p}}{\partial x} = 0 \tag{14}$$

$$\left(D_{2,eff}\frac{\partial c_2}{\partial x}\right)_{sep} = \left(D_{2,eff}\frac{\partial c_2}{\partial x}\right)_p \tag{15}$$

At $x = L$:

$$\frac{\partial \phi_{1,p}}{\partial x} = -\frac{I_{app}}{\sigma_{p,eff}} \tag{16}$$

3. Simulation of the cycling performance

Simulation of each cycle consists of three steps. Charging is carried out at constant current until the cutoff voltage for charge (4.2 V) is reached and then the cell is charged in the constant voltage mode, until the current drops to 50 mA. It is then followed by discharge at a constant current until the cutoff voltage for discharge (3.0 V) is reached. During the simulation of cycling performance, the model is solved repeatedly maintaining all parameters at constant values (as shown in Table 2). The fade in capacity with cycling is brought about by the additional side reaction flux ($J_{s,n}$), the increase in film thickness over time and the resultant change in the anodic overpotential. The solution of the model equations for simulating the cycling performance is different from that of a single discharge curve in that there arise numerical inconsistencies between values the variables solved for at the time between two consecutive steps. For example, the set of values for the dependent variables obtained at the end of a discharge step does not always provide consistent initial values for those variables at the beginning of the next charge step. This issue has been discussed in detail by Wu and White [22]. As recommended by these authors an indigenous initialization subroutine DAEIS [22] is used to address this numerical inconsistency. The solution of the model equations is carried out using the FORTRAN solver DASRT [21]. For each approach, the corresponding set of model equations presented in Table 1 are solved repeatedly to predict the profile of the cell voltage as a function of time for 800 cycles.

Table 2
List of parameters (all values are from Ref. [17] unless otherwise stated)

Symbol	Anode	Cathode	Separator
σ (S m^{-1})	100	100	
ε_1	0.49	0.59	
ε_2	0.485	0.365	0.724
brug	4.0	4.0	4.0
D_1 (m^2 s^{-1})	3.9e−14	1.0e−14	
D_2 (m^2 s^{-1})	7.5e−10	7.5e−10	7.5e−10
k ((A m^{-2} mol m^{-3})$^{3/2}$)	4.854e−6	2.252e−6	
c_1^{max} (mol m^{-3})	30555	51555	
$c_{1,0}$ (mol m^{-3})	0.03 × 30555	0.95 × 51555	
$c_{2,0}$ (mol m^{-3})	1000	1000	1000
R_j (m)	2e−6	2e−6	
L_i (m)	88e−6	80e−6	80e−6
$\phi_{2,0}$	0	0	0
$U_{ref,s}$ (V)	0.40		
R_{SET} (Ω m^{-2})	0.01		
$i^0_{j,side}$ (A m^{-2})	1.0e−11[a]		
$M_{s,j}$ (kg mol^{-1})	7.3e−4		
$\rho_{s,j}$ (kg m^{-3})	2.1e−3		
$\kappa_{s,j}$ (S m^{-1})	1.0e−2[a]		
A_j (m^{-2})	603.06e−6	531.3e−6	
α	0.5	0.5	
t^+	0.363	0.363	
F (C mol^{-1})	96487		
R (J mol K^{-1})	8.314		
T (K)	298.15		

[a] Assumed.

4. Results and discussion

The validity of the parabolic approximation has been established by Wang et al. [9] and Subramanian et al. [10], and hence is not repeated here. As shown in Ref. [10], the approximation is very efficient for low to moderate rates of discharge. There are two possible limitations that may arise to this approximation. Under very high rates of discharge, the approximation of the concentration profile inside a spherical particle with a second-degree polynomial is not sufficiently accurate. To address this limitation, Subramanian et al. [10] recommended higher order approximations of the concentration profile. The second limitation arises from the inability of the approximation to capture the concentration profile at very short times accurately. Wang and Srinivasan [23] suggested an empirical correction factor to the average concentration ($c_{s,j}$) that is obtained from Eqs. (6)–(8) to simulate the transient profile of the concentration more accurately.

Fig. 2a shows the discharge profile obtained from all the three models at 0.2C as well as 1C rates of discharge. As observed at rates as low as 0.2C, both the approximate models (SP and PP) provide a very accurate profile. This figure validates the PP as well as the SP model independently. Both these models compare well with the rigorous P2D model. There is almost negligible deviation of the predictions from the SP model from those of the porous electrode-based models. The absolute values of the percentage of error between the PP and the P2D models as well as those between the SP and the P2D models are shown in Fig. 2b on a logarithmic scale. These show that the SP model is as valid as the porous electrode models for discharge rates as high as 1C. As observed from this figure, the error between the PP and the rigorous P2D model is of the order of 1e−5 for the 0.2C rate. This establishes the validity of the polynomial approximation even in a sophisticated porous electrode model. The set of parameters used to obtain these curves is presented in Table 2. Fig. 3 shows the discharge curves predicted from the SP and the PP models for fresh as well as 800 cycles at the 0.2C rate. The good degree of fit between the predictions of both the models not only reinstates the results from Fig. 2, but also justifies the claim that the SP approach is quite successful in simulating the cycling performance of a cell as much as a rigorous model based on the porous electrode theory.

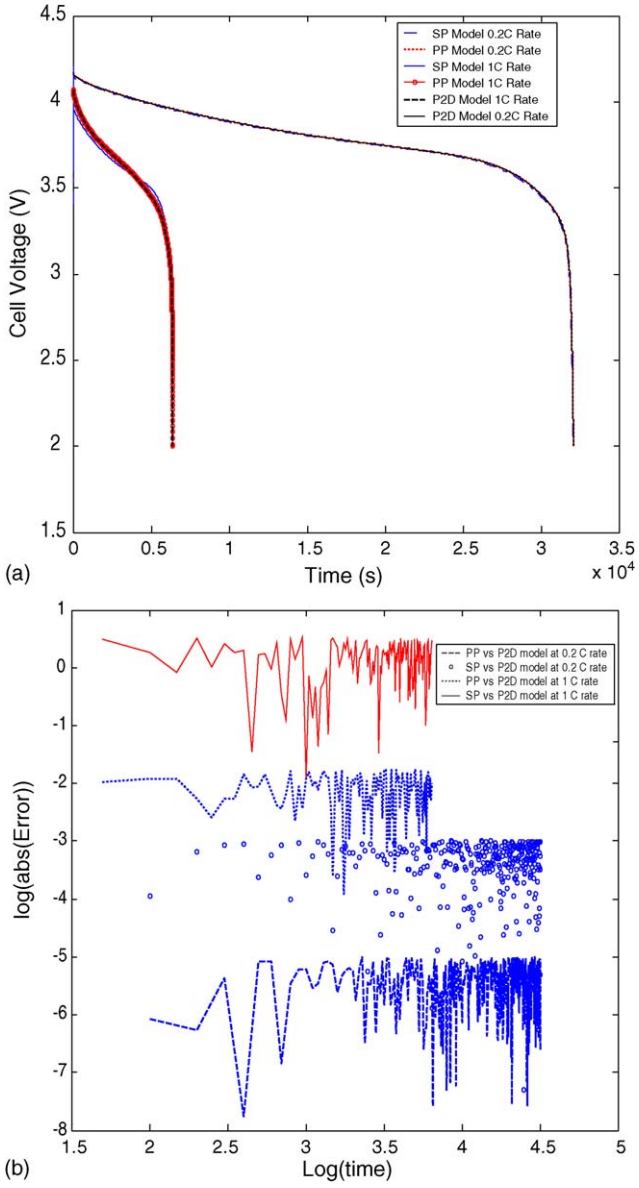

Fig. 2. (a) Validation of the SP and the PP models. (b) Comparison of the error between the approximate models (PP and SP) and the rigorous model (P2D) at various rates of discharge.

Table 3
Comparison of the PP and the SP models with the P2D model

Rate of discharge	Percentage error between the PP and the P2D models		Percentage error between the SP and the P2D models	
	Cycle 1	Cycle 800	Cycle 1	Cycle 800
0.2C	1e−5	4e−5	1e−3	2.42e−2
1C	0.175	1.112	3.404[a] 3.450[b]	6.70[a] 7.12[b]
2C	0.013	0.135	59.37[a] 37.30[b]	67.43[a] 47.05[b]

[a] With parameters from Table 2.
[b] With modified parameters (see text).

The limitations of the SP model as compared to the porous electrode approach are presented in Fig. 4. The discharge curves at higher rates are shown for cycle 1. Despite the good agreement with the porous electrode models until the 1C rate there is a significant deviation at higher rates. Table 3 presents the total error out of the SP and the PP approaches as compared to the P2D approach, for various rates at cycle 1 and 800. The vast difference between the profiles predicted for the 2C case is, however, expected. During low rates of discharge the limitations from the solution phase are not as significant as those presented by the solid phase. Hence, the assumption that the solution phase limitations are negligible stated in Section 2.3 is not violated under these conditions. The solid phase is treated alike in the PP as well as the SP model; so, the difference between the two models is virtually negligible at the 0.2C rates. However, at rates of discharge as high as 2C, not only are the restrictions posed by the transport in the solution phase important [24], but also the dependence of the kinetic expression on the solution phase concentration is significantly different for the two models. Whereas the PP model follows the change in the solution phase concentration via the material balance in the solution phase, the SP model assumes the concentration to be constant throughout discharge. This is reflected in the difference in the slope of the discharge plateaus between the two models in Fig. 4. Note that no such difference is observed between the two models at the 0.2C rate in Fig. 1, which substantiates the assumption that the contribution of the solution phase is not significant at rates of discharge below 1C. To validate the argument that the difference between the PP and the SP models at higher rates is because of the solution phase limitations, the solution phase conductivity (κ_{eff}) was increased by a factor of two and the solution phase diffusion coefficient ($D_{2,\text{eff}}$) was set to a very high value (1e−3 $\text{m}^2\,\text{s}^{-1}$) in the PP model. The revised profiles are also shown in Fig. 4. As observed, at 1C rate the change is minimal. However, at the 2C rate, the revised profile shows a better agreement with the SP model; still a complete agreement between the two models is not obtained, since the value for the solution phase concentration in the kinetics expression continues to be a constant. The significance of the change in the solution phase concentration is illustrated in Fig. 5. Whereas for discharge rates up to 1C the change in the solution phase concentration is less than 10%, for the 2C rate it is as high as 40%. The SP model completely

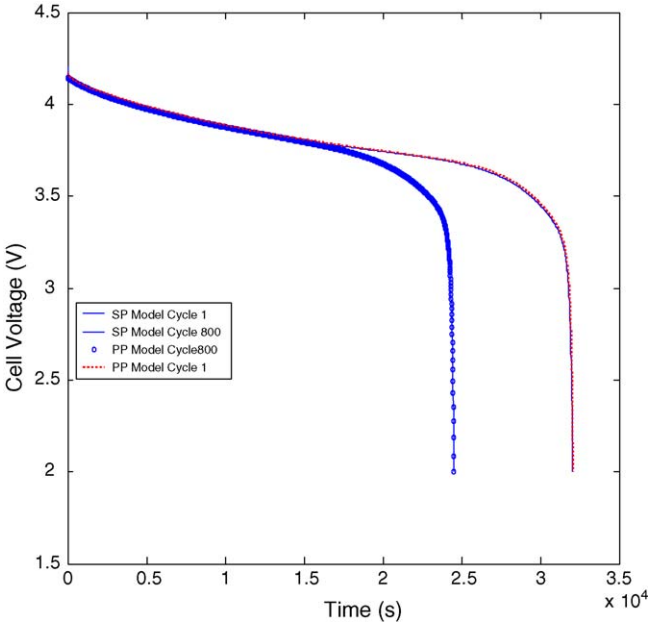

Fig. 3. Comparison of the prediction of the cycling performance from the PP and SP models at 0.2C rate.

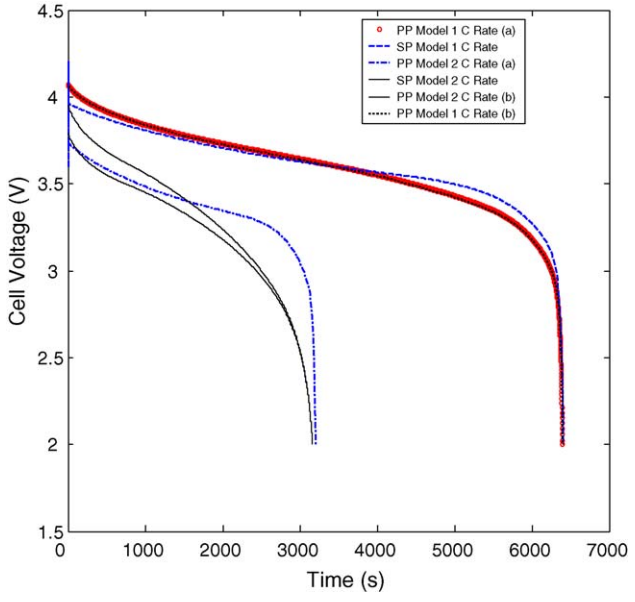

Fig. 4. Comparison of the discharge curves predicted from the PP and SP models at higher rates: (a) with parameters from Table 2 (b) with modified parameters (see text).

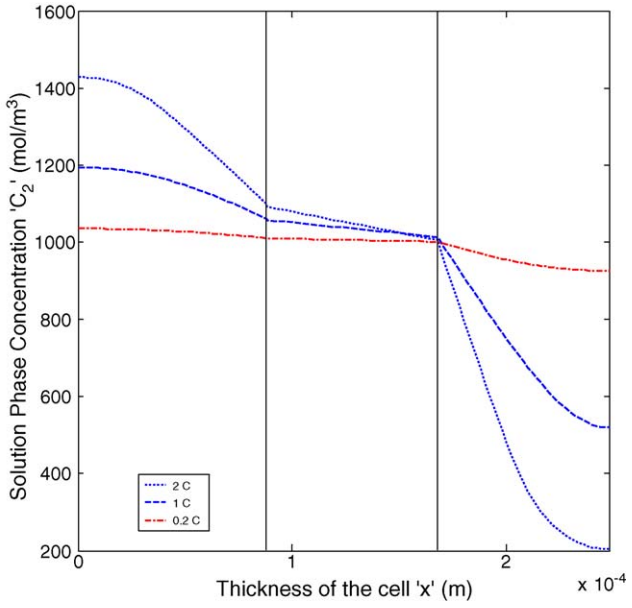

Fig. 5. Change in the solution phase concentration at various rates of discharge as predicted by the PP model.

ignores the changes in the solution phase concentration, and hence is incapable of predicting the discharge profile in the kinetics dominated regime. An alternate discussion is provided by Botte and White [25], wherein the inclusion of the activity coefficient term in the solid phase was suggested to improve the predictions at high rates.

The computational time for 800 cycles for all the three approaches is presented in Table 4. Hundred node points were used to approximate each coordinate using the three-point finite differences scheme for each electrode in the P2D and the PP models. The SP model has a distinct advantage over the porous electrode models, in terms of the computational time, despite its limitations in terms of accuracy at higher rates. Nevertheless, the PP model exhibits a good efficiency both in terms of accuracy as well as computational time, as observed from Tables 3 and 4. The incorporation of the parabolic approximation [9–11] reduces the computational time by at least 70%. The choice of DASRT coupled with DAEIS is found to be a robust solver suitable for solving the models repeatedly during the simulation of the cycling performance of the cell, and hence is ideal for capacity fade analysis. DASRT [21] is a variable time step solver with an in built zero crossing detection feature. This feature of DASRT, along with appropriate constraints, enables one to interpolate to the exact time of transition from one step to another (charging to discharging, for example). The capabilities of DAEIS are addressed by Wu and White [22].

Table 4
Comparison of the computational cost for the three models

Model	CPU time for 800 cycles (s)
P2D	1.12e5
PP	9600
SP	27

5. Conclusion

Two approximate models (SP and PP) were used to simulate capacity fade in lithium ion batteries and compared to a complete model (P2D). Both of the approximate models compared well with the P2D model up to 1*C* rate of discharge. Incorporation of the parabolic approximation for the solid phase concentration of the diffusing species significantly reduces the computational time as compared to the P2D model for both the SP and the PP models, while still retaining sufficient accuracy as reported by Subramanian et al. [10], even for a complex sandwich model. The low solution time as well as a high degree of accuracy identifies these models as suitable for simulating the cycling performance of a cell, when the model equations are solved over and over. The SP models neglects solution phase limitations, and hence is not accurate at rates beyond 1*C*, when concentration gradients in the liquid phase become the limiting factor. While the SP model can be used successfully to simulate the cycling of lithium ion batteries up to the 1*C* rate, the PP model is best suited for rates higher than 1*C*, since there is no significant loss of accuracy and at the same time the computational time is greatly reduced. DASRT is identified as the suitable choice of solver due to its robustness in solving the model equations over 800 cycles.

Acknowledgement

The authors gratefully acknowledge the financial support from the National Reconnaissance Office (NRO) under contract # NRO-000-03-C-0122.

References

[1] K.E. Thomas, J. Newman, R.M. Darling, in: W.A. van Schalkwijk, B. Scrosati (Eds.), Advances in Lithium-Ion Batteries, Kluwer Academic/Plenum Publishers, NY, 2002, pp. 345–392.
[2] G.G. Botte, V.R. Subramanian, R.E. White, Electrochim. Acta 45 (15–16) (2000) 2595–2609.
[3] P.M. Gomadam, J.W. Weidner, R.A. Dougal, R.E. White, J. Power Sources 110 (2) (2002) 267–284.
[4] P. Arora, R.E. White, M. Doyle, J. Electrochem. Soc. 145 (1998) 3543–3553.
[5] T.F. Fuller, M. Doyle, J. Newman, J. Electrochem. Soc. 141 (1) (1994) 1–10.
[6] M. Doyle, J. Newman, J. Power Sources 54 (1995) 46–51.
[7] M. Doyle, J. Newman, J. Appl. Electrochem. 27 (1997) 846–856.
[8] G. Sikha, B.N. Popov, R.E. White, J. Electrochem. Soc. 151 (7) (2004) A1104–A1114.
[9] C.Y. Wang, W.B. Gu, B.Y. Liaw, J. Electrochem. Soc. 145 (1998) 3407.
[10] V.R. Subramanian, D. Tapriyal, R.E. White, Electrochem. Sol. State Lett. 7 (9) (2004) A259–A263.

[11] M. Ozisik, Boundary Value Problems of Heat Conduction, Dover Publications, NY, 1968.
[12] B.S. Haran, B.N. Popov, R.E. White, J. Power Sources 75 (1) (1998) 56–66.
[13] G. Ning, B.N. Popov, J. Electrochem. Soc. 151 (10) (2004) A1584.
[14] Q. Guo, R.E. White, private communication.
[15] P.K. Adanuvor, R.E. White, J. Electrochem. Soc. 135 (8) (1988) 1888–1898.
[16] V.R. Subramanian, J.A. Ritter, R.E. White, J. Electrochem. Soc. 148 (11) (2001) E444–E449.
[17] P. Ramadass, B. Haran, P.M. Gomadam, R.E. White, B.N. Popov, J. Electrochem. Soc. 151 (2) (2004) A196–A203.
[18] M.W. Verbrugge, B.J. Koch, J. Electrochem. Soc. 143 (2) (1996) 600–608.
[19] M.W. Verbrugge, J. Electrochem. Soc. 139 (12) (1992) 3529–3535.
[20] P. Ramadass, Ph.D. Thesis, University of South Carolina, 2003.
[21] L.R. Petzold, SIAM J. Sci. Stat. Comp. 3 (1982) 367.
[22] B. Wu, R.E. White, Comput. Chem. Eng. 25 (2–3) (2001) 301–311.
[23] C.Y. Wang, Srinivasan, J. Power Sources 110 (2002) 364–376.
[24] P. Arora, M. Doyle, A.S. Gozdz, R.E. White, J. Newman, J. Power Sources 88 (2000) 219–231.
[25] G.G. Botte, R.E. White, J. Electrochem. Soc. 148 (1) (2001) 54–66.